Effect of Natural and Organically Modified Montmorillonite Clays on the Properties of Polydimethylsiloxane Rubber

Manuela L. Q. A. Kaneko, Inez V. P. Yoshida

Instituto de Química, Universidade Estadual de Campinas, CP 6154, 13084-971, Campinas, São Paulo, Brazil

Received 29 May 2007; accepted 18 December 2007
DOI 10.1002/app.27898
Published online 20 February 2008 in Wiley InterScience (www.interscience.wiley.com).

ABSTRACT: The effects of natural (MT) and organically modified (O-MT) montmorillonite clays on the properties of polydimethylsiloxane (PDMS) rubber were evaluated. Rubber composites with different clay contents were prepared by a compounding procedure in an open two-roll mill, which was followed by a compression-molding step in which the PDMS matrix was peroxide crosslinked. The clay rubber composites were characterized by swelling measurements in toluene, thermogravimetric analyses, X-ray diffraction, scanning electron microscopy, and tensile tests. The introduction of MT restricted the solvent swelling and increased the crosslinking density of the rubber, which indicated the formation of a covalent filler–matrix interface. The enhanced interaction between MT and PDMS reduced the aggregation size of MT particles in the MT composites and promoted an increase in the separation of the clay layers. When the rubber was filled with O-MT, a higher solvent amount was incorporated in the material, and this trend increased with the clay content. Moreover, the low interaction between O-MT and the PDMS chains resulted in larger clay aggregates in the O-MT composites compared to those with MT. Despite the different interface natures, both clays enhanced thermal stability and acted as reinforcing fillers in relation to Young's modulus and tensile strength. © 2008 Wiley Periodicals, Inc. J Appl Polym Sci 108: 2587–2596, 2008

Key words: composites; mechanical properties; organoclay; polysiloxanes; rubber

INTRODUCTION

The wide industrial use of polysiloxane rubbers arises from a combination of the unique properties presented by these elastomers, such as their low-temperature flexibility, excellent thermal and oxidative stabilities, low surface tension, chemical inertness, and good dielectric properties. Polysiloxane elastomeric networks also remain elastic over a wide range of temperatures, which makes them suitable for a variety of engineering applications, especially under unusual service conditions.[1–3]

Polydimethylsiloxane (PDMS) is the most prevalent member of this class of materials, but its mechanical properties in the unfilled state are poor.[2,3] Usually, PDMS elastomers require the use of particulate fillers to obtain the reinforcement desired for the majority of applications. PDMS networks are often reinforced with silica particles, and the interaction between the matrix and filler is mainly ensured by a covalent silica–PDMS interface or by hydrogen bonds between silanol groups from the silica surface and the oxygen atoms from the polymer chains.[4] The effects of other particulate fillers, such as mica flakes,[5] biogenic silica, and eucalyptus fibers,[6,7] in PDMS rubber have also been studied. Moreover, increasing attention has been paid to PDMS–clay composites,[8–12] although a few researchers[10,13] have reported that different kinds of clay have dissimilar influences on PDMS microcomposite properties.

This study focused on an investigation of the effect of natural (MT) and organically modified montmorillonite (O-MT) clays on the thermal stability, morphology, and mechanical properties of PDMS rubber composites derived from a high-molar-mass (10^6 g/mol) PDMS matrix. As shown in a forthcoming article, nanolayer dispersion can be achieved in high-molar-mass PDMS matrices without solvent assistance or high shearing. However, an understanding of microcomposite behavior, regardless of the type and content of clay, is crucial for the development of nanocomposites, mainly because the reinforcement of rubbers with layered silicates is far more complicated than that with silica or carbon black because of their unique structure and interaction behavior with the rubber matrix.

Correspondence to: I. V. P. Yoshida (valeria@iqm.unicamp.br).

Contract grant sponsor: Fundação de Amparo à Pesquisa do Estado De São Paulo (FAPESP); contract grant number: 03/09926-1.

Contract grant sponsor: Conselho Nacional de Desenvolvimento Cientifico e Tecnológico (CNPq); contract grant number: 473670/2004-6.

EXPERIMENTAL

Materials

Two montmorillonite clays were used in this study: MT and O-MT. The MT, GELMAX 400, supplied by Eduardo Vasconcelos Representações, Ltd. (Porto Alegre, Brazil), was a polycationic clay with cation exchange capacity of 106 mequiv/100 g and a real density of 1.54 g/cm^3. The O-MT was purchased from Bentec (Livorno, Italy), and it was commercially available as Viscogel ED. Viscogel ED (O-MT) was a montmorillonite clay modified by long-chain quaternary alkyl ammonium salts, which increased the clay gallery distance and made it compatible with hydrophobic polymers. Polydimethylsiloxane gum (PDMS-gum), with an average molar mass of approximately 10^6 g/mol and a ($SiCH_3CH{=}CH_2O$) : [$Si(CH_3)_2O$] $<$ 1 : 1000 molar ratio, was used as a polymeric matrix for the rubbers. It was supplied by Dow Corning do Brazil, Ltd. (Hortolândia, Brazil). The 2,5-dimethyl-2,5-di(*tert*-butylperoxy)hexane used as a radical initiator agent was obtained from Akzo Nobel Polymer Chemicals (Amersfoort, The Netherlands). Toluene was acquired from Synth (Diadema, Brazil), and it was used as received.

Preparation of the clay–rubber composites

The clay–rubber composites were prepared with 5, 10, 20, and 30 phr (parts per hundred parts of rubber by weight) of MT or O-MT, previously dried for 24 h in a vacuum oven at 80°C and 10^{-1} torr and with 0.65 phr of peroxide. A reference rubber sample was also prepared by the mixture of PDMS-gum with peroxide, and it was referred to as unfilled silicone rubber (USR). The compounding procedure of the samples was carried out in a COPÉ open two-roll mill (Novo Hamburgo, Brazil) for 20 min at 25°C. The rotors were operated at a speed ratio of 1 : 1.4. The compounds were compression-molded in a Parabor PL350 compression molding machine (São Paolo, Brazil) at 175°C and 22 MPa of pressure for 10 min, followed by a postcure treatment in a vacuum oven at 120°C for 8 h. The samples were molded as 150 $\times$ 150 $\times$ 2-mm^3 sheets. Two sets of silicone rubber (SR) composites were obtained: the first one with natural montmorillonite (MT/SR) and the second one with organically modified montmorillonite (O-MT/SR).

Characterization of the clay powders and clay–rubber composites

MT and O-MT clay powders were characterized by Brunauer–Emmett–Teller surface area measurements in a Micromeritics Flow Sorb II-2300 (Norcross, GA). Their elemental compositions were determined by energy dispersive X-ray fluorescence (XRF) in a Shimadzu (Kyoto, Japan) EDX-700 instrument, with a rhodium tube and a Si(Li) detector. IR spectra of MT, O-MT, and the clay–rubber composites were obtained in a Bomem MB-SERIES spectrometer (Waltham, MA) in KBr pellets; we collected 256 scans from 4000 to 400 cm^{-1}, with a resolution of 4 cm^{-1}. X-ray diffraction (XRD) measurements of these materials were carried out in a Shimadzu XRD6000 instrument equipped with Cu Kα radiation (λ = 0.15418 nm, where λ is the wavelength), with 30 mA of current and 40 kV of voltage. The clays were dried in a vacuum oven at 100°C for 8 h before the characterization.

The swelling measurements of the rubbers were performed in toluene following ASTM D 471.[14] Rubber strips with dimensions of 20 $\times$ 10 $\times$ 2 mm^3 were weighed and immersed in 25 cm^3 of the solvent. At regular intervals, the surface of the swollen strip was gently dried with filter paper, and the weight of the samples was registered. This procedure was repeated until a constant swollen weight was obtained. Afterwards, samples were dried in a vacuum oven at 50°C for 24 h and weighed again. For each rubber, three specimens were tested, and the average results are reported.

The thermal stability of the rubbers was analyzed by thermogravimetric analysis (TGA) in a TA 2950 thermobalance (TA Instruments, New Castle, DE) from 30 to 1000°C at a heating rate of 20°C/min under an argon flow (100 cm^3/min, 99.999%).

The morphology of the rubbers was studied by scanning electron microscopy (SEM) in a Jeol JSM-6360 LV microscope (Middleton, WI) operated at 20 kV. The rubber samples were cryogenically fractured, and the fracture surface was sputter-coated with very thin carbon and gold layers before they were scanned in a Bal-Tec MED 020 instrument (Balzers, Liechtenstein).

The tensile properties of the rubbers were determined in an EMIC 2000 tensile tester (São José dos Pinhais, Brazil) according to ASTM D 412-98a[15] at 25°C with a 500 N-load cell and a crosshead speed of 500 mm/min. All tests were evaluated with at least seven specimens considered for each composition, and the average results were reported. Specimens were conditioned at 23°C and 50% relative humidity for 24 h before the testing.

RESULTS AND DISCUSSION

Characterization of the clay powders

The MT diffractogram (not shown) presented a single (001) diffraction peak at 2θ = 7°, corresponding to a *d*-spacing (interlayer distance) of 12.6 Å, calculated according to Bragg's equation: $\lambda = 2d \sin\theta$ (where *d* is the *d*-spacing and θ is the diffraction angle). Other diffraction peaks, with characteristic intensities at 2θ = 20, 35, and 72°, corresponding to the (100), (110), and (060) smectite plane reflections,[16]

TABLE I
Elemental Compositions[a] of MT and O-MT

	Chemical composition (wt %)	
	MT	O-MT
SiO_2	60.8	64.6
Al_2O_3	27.4	26.7
K_2O	3.0	0.6
CaO	2.9	1.2
MgO	2.7	—
Fe_2O_3	2.4	6.3
Others	0.8	0.6

[a] Obtained from the equipment. This does not correspond to the real compounds.

respectively, were also observed. In addition, some residual impurities corresponding to the basal plane reflections of quartz ($2\theta = 27^\circ$), cristoballite ($2\theta = 22^\circ$), and illite ($2\theta = 9.4^\circ$) were also detected. The O-MT diffractogram (not shown) presented diffraction peaks at 2.8, 5, and 7.5° corresponding to *d*-spacings of 31.6, 17.6, and 11.8 Å, respectively. The basal reflection at $2\theta = 5^\circ$ was explained by layer–layer interference (second-order reflection),[17] and the basal reflection at $2\theta = 7.5^\circ$ ($d = 11.8$ Å) indicated that part of the clay layers were not expanded and remained in their pristine state.

MT and O-MT showed low surface areas, 28.36 and 3.08 m^2/g, respectively. The estimated value of the Brunauer–Emmett–Teller surface area found for MT agreed with values reported in the literature.[18–21] This value represented the external surface of the clay particles and did not include the effective area of the galleries, estimated as 620 m^2/g.[21,22] The lower surface area of O-MT reflected the clay modification with the alkyl ammonium cations. As the voids between primary particles (micropores) and aggregates (mesopores) were filled with the organic cations, they made the transport of N_2 molecules difficult.[23,24]

The elemental composition of these clays, obtained by XRF and expressed as percentage of oxides, are shown in Table I. They were composed essentially of silica and alumina (>80%), as expected, with small concentration of other oxides. The XRF analyses also showed the presence of Mg^{2+}, K^+, Ca^{2+}, and Fe^{3+} in the MT samples, probably as interlayer cations.

The IR spectra for MT and O-MT are shown in Figure 1. Both samples were characterized by absorptions at 1089, 1024, and 461 cm^{-1} related to Si—O—Si groups and absorptions at 517 cm^{-1} related to Al—O—Al groups. Other absorptions at about 3435 and 1643 cm^{-1}, related to the adsorbed water, were also observed. Weak bands at 779 and 630 cm^{-1} were associated with quartz and cristoballite, respectively, in agreement with the XRD results. The MT spectra also showed absorption at 836 cm^{-1}, characteristic of AlOMg, which indicated that Mg^{2+} was located in the octahedral sites.[25] In the spectrum

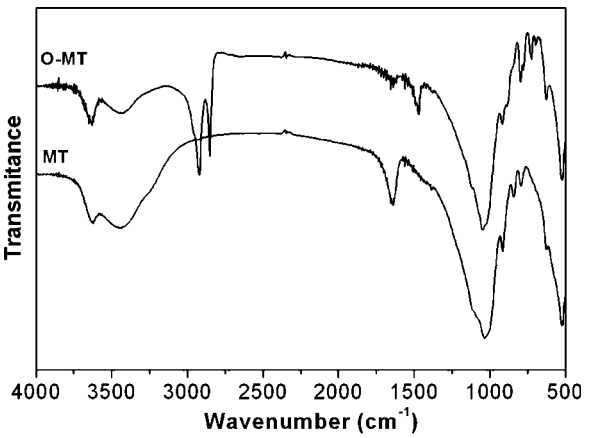

Figure 1 IR spectra for MT and O-MT.

of O-MT, absorptions related to alkyl ammonium, especially to the CH_2 group at 2917 and 2851 cm^{-1}, were also observed.[26]

The TGA curves and their derivatives for the MT and O-MT samples are shown in Figure 2. Two main stages of weight loss were observed for MT. The first (35–200°C), with a loss of 2.7%, was attributed to the presence of weakly bonded water and water intercalated into the interlayer regions. The second stage (400–750°C) was related to the loss of structural hydroxyl groups.[27–29] In this stage, the TGA curve indicated that the dehydroxylation process occurred in different steps, with maximum rates at 566, 599, and 640°C. This result reflects the different crystallographic locations of the hydroxyl groups in the clay structure.[30] O-MT curves showed the absence of weakly bonded water, which indicated the hydrophobic character of this clay, and its thermal stability up to 200°C. The decomposition of alkyl ammonium cations present in the O-MT clay was observed from 200 to 450°C. The organic cation contents in the interlayer region and between the aggregates, estimated from this temperature range, corresponded to 32 wt %. The multiple peaks in the

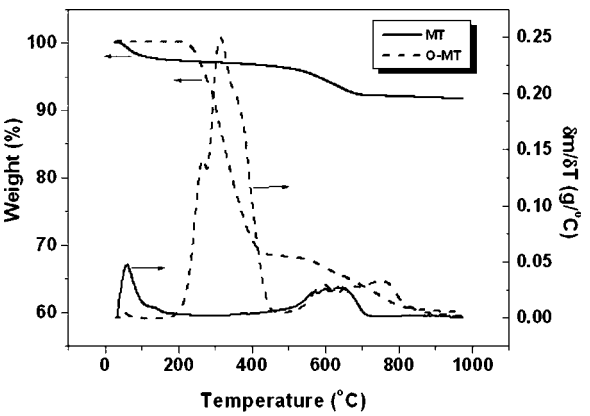

Figure 2 Thermogravimetry and DTG (δm/δT) curves for MT and O-MT.

differential thermogravimetry (DTG) curve of O-MT indicated that the organic component was evolved in distinct steps. The first step was associated with the volatilization of the excess of the organic cations located outside the galleries; the second and third steps were related to the degradation of the organic cation bonded into the clay layers.[29] Between about 500 and 950°C, the dehydroxylation process and the volatilization of the residual organic component produced about 60% inorganic residue.[29,30]

Swelling measurements of the clay–rubber composites

The effects of MT and O-MT on the swelling properties of the PDMS rubber were evaluated. The swelling measurements, performed in toluene, allowed the determination of the swelling ratio (S_R), the average molar mass between crosslinking points (M_C), and the crosslinking density of the polymeric network (n^{FR}) of the composite samples.

We calculated S_R, discounting the amount of filler in each sample, by using eq. (1):[4]

$$S_R = \frac{[m_S - (\alpha_{filler} m_d)]}{(\alpha_{pol} m_d)} \quad (1)$$

where m_s is the weight of the swollen sample at equilibrium, m_d is the weight of the dried sample after swelling, and α_{filler} and α_{pol} are the filler and polymer weight fractions, respectively. The curves of S_R as a function of time are shown in Figure 3.

The MT/SR composites showed smaller equilibrium swelling ratios [$S_{R(eq)}$'s] compared to the USR, whereas the O-MT composites showed the opposite behavior. When the SR was filled with O-MT, a higher solvent amount was incorporated into the rubber composite, and this trend increased with the O-MT content, in contrast to the results with MT.

M_C was calculated with the Flory–Rehner equation [eq. (2)] for a tetrafunctional polymeric network model:[31]

$$M_C = \frac{[-d_{pol} V_{sol} (\varphi_{pol}^{1/3} - \varphi_{pol}/2)]}{[\ln(1 - \varphi_{pol}) + \varphi_{pol} + \chi \varphi_{pol}^2]} \quad (2)$$

where d_{pol} is the density of PDMS-gum, V_{sol} is the molar volume of toluene, Φ_{pol} is the volume fraction of the polymer in the swollen sample at equilibrium, and χ is the Flory–Huggins polymer–solvent interaction parameter. Φ_{pol} was calculated by eq. (3):[32]

$$\frac{1}{\varphi_{pol}} = 1 + S_{R(eq)} \frac{d_{pol}}{d_{sol}} \quad (3)$$

where d_{sol} is the density of toluene at 40°C. χ was determined by eq. (4):[32,33]

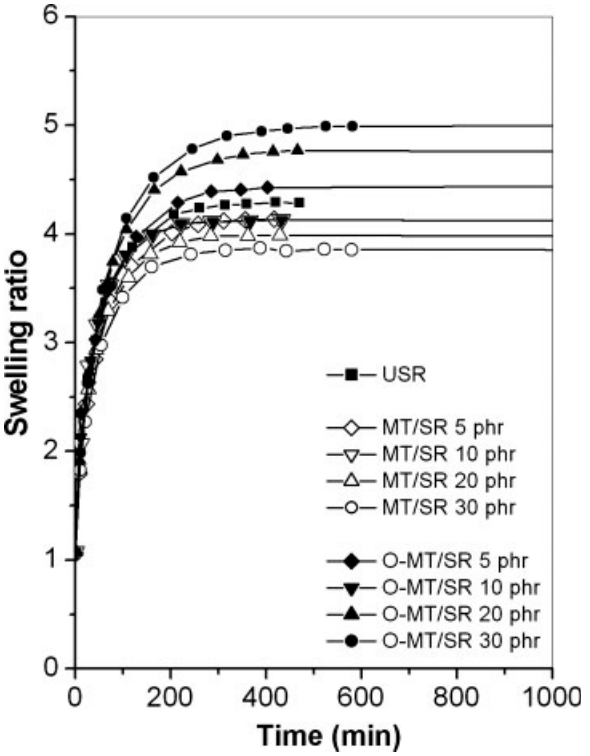

Figure 3 Variation of S_R with time for the swelling of the USR and SR composites in toluene.

$$\chi = \frac{(\delta_{sol} - \delta_{pol})^2}{RT} V_{sol} \quad (4)$$

where δ_{sol} and δ_{pol} are the solubility parameters of the solvent and polymer, respectively; R is the gas constant; and T the absolute temperature. M_C values obtained for each sample allowed the calculation of n^{FR} with eq. (5):[34]

$$n^{FR} = \frac{d_{pol}}{M_C} \quad (5)$$

The $S_{R(eq)}$, M_C, and n^{FR} values calculated from the swelling measurements of the samples in toluene are presented in Table II.

According to the results obtained, the addition of MT to the PDMS matrix promoted an increase in the crosslinking density of this matrix, which contributed to a decrease in the M_C and $S_{R(eq)}$ values. This fact suggested the formation of a covalent MT–PDMS interface. The Si—OH groups present on the MT platelet surface could have acted as nucleophiles to the Si atoms of the PDMS main chains, which promoted chain scission and the formation of shorter PDMS chains with $Si(CH_3)_2OH$ end groups. These chain fragments could then interact with other silanol groups from other PDMS chains or even with the Si—OH of the MT platelet surface to reduce the average molar mass between the nodes of the

TABLE II
$S_{R(eq)}$, n^{FR}, and M_C Values for the Rubbers in Toluene

Sample	$S_{R(eq)}$	n^{FR} (10^{-4} mol/cm^3)	M_C (g/mol)
USR	4.31 (0.10)	2.15 (0.08)	3381 (137)
MT/SR 5 phr	4.14 (0.01)	2.31 (0.01)	3146 (15)
MT/SR 10 phr	4.11 (0.02)	2.35 (0.02)	3101 (27)
MT/SR 20 phr	3.97 (0.03)	2.50 (0.03)	2916 (41)
MT/SR 30 phr	3.85 (0.04)	2.63 (0.04)	2771 (45)
O-MT/SR 5 phr	4.49 (0.10)	2.00 (0.08)	3628 (150)
O-MT/SR 10 phr	4.73 (0.35)	1.85 (0.20)	3980 (525)
O-MT/SR 20 phr	4.76 (0.34)	1.83 (0.24)	4020 (489)
O-MT/SR 30 phr	4.98 (0.02)	1.67 (0.01)	4354 (38)

Standard deviations are given in parentheses.

network and increase its crosslinking density, especially in the vicinity of the clay particles. The increase observed in the crosslinking density of the MT/SR composites with clay content was a consequence of an increase of the amount of Si—OH groups on the platelet surface available for covalent bonds. The O-MT/SR composites showed lower crosslinking density than the USR and MT/SR composites. This result suggests that in O-MT, the presence of alkyl ammonium cations restricted the formation of nodes in the PDMS network of the O-MT filled composites. This behavior was not usual but could be justified by the partial absorption of the radical initiator on the filler surface. The investigations reported by Song et al.[35] and Chang et al.[36] also showed similar results or trends in the crosslinking of poly(styrene-*co*-butadiene) rubber and (ethylene–propylene) rubber, respectively, both reinforced with organic clay. The interlayer distance of O-MT (31.6 Å) was greater than that of MT (12.6 Å). This fact, associated with the chemical similarity between the radical initiator and the O-MT surface, led to the absorption of the peroxide into the O-MT clay galleries. As a result, the radical initiator was reduced in the rubber, which lowered the crosslinking density. In addition, O-MT showed higher amounts of Fe^{3+} than MT, which contributed to the capture of free radicals, with the consequent blockage of the crosslinking process by the reaction $Fe^{3+} + R^{\bullet} \rightarrow Fe^{2+} + R^{+}$.[37]

Thermal stability of the clay–rubber composites

The thermal stability of the rubbers was evaluated by TGA, and the thermogravimetric curves for USR and SR composites are shown in Figure 4. USR showed good thermal stability, with an initial temperature of weight loss at approximately 400°C. One decomposition step of thermal degradation was observed, with the temperature of the maximum degradation rate (T_{max}) around 500°C. It is well

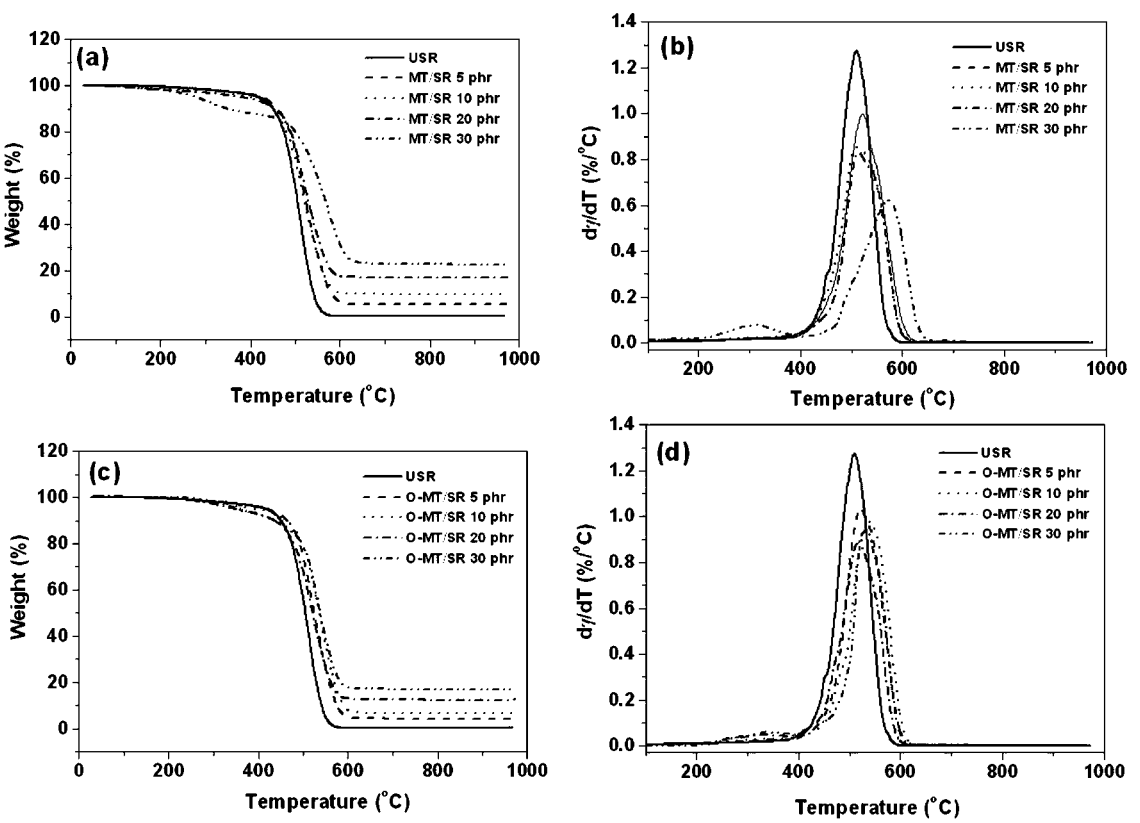

Figure 4 (a) Thermogravimetry and (b) DTG curves for the USR and MT/SR composites and (c) thermogravimetry and (d) DTG curves for the USR and O-MT/SR composites.

known that the thermal degradation of the linear PDMS chain under an inert atmosphere involves the formation of volatile cyclic oligomers by intrachain or interchain rearrangements.[38]

For the MT/SR composites, the presence of MT contributed to a lower rate and broader degradation process, with an increase in T_{max} values compared to USR, which indicated a slight stabilizing effect of this clay on PDMS chain degradation. This was in contrast to the results described by Osman et al.[5] for montmorillonite/PDMS vinyl-terminated composites, where the montmorillonite enhanced the thermal degradation of PDMS. The improvement in the thermal stability of the MT/SR composites could be attributed to the increase in the crosslinking density, which restricted the mobility of the PDMS chains and hindered their intermolecular and intramolecular rearrangements.[6,39,40] However, in the MT/SR composite with 30-phr composition, there was a first degradation step between 200 and 400°C, which corresponded to a 10 wt % loss. Probably, in this composition, the amount of Si—OH groups from the platelet surface of the clay promoted a more intense degradation of the PDMS chains, which gave rise to shorter PDMS chains with $Si(CH_3)_2OH$ end groups, in agreement to the results observed in the swelling measurements. In the PDMS–$Si(CH_3)_2OH$ end groups, the initial degradation temperature was shifted to lower values due to the characteristic depolymerization promoted by the backbiting of the silanol to the siloxane chain.[41] However, the main degradation step showed T_{max} at a higher temperature, about 580°C, as was observed for the composite filled with 30 phr of MT clay [Fig. 4(a,b)].

The O-MT/SR composites showed a low-intensity degradation step in the 230–427°C range, which was assigned to the degradation of the alkyl ammonium cation,[42] and a principal degradation step in the 427–600°C range, which was associated with the degradation of the PDMS matrix [Fig. 4(c,d)]. O-MT promoted a small effect on the degradation rate in relation to MT.

X-ray characterization of the clay–rubber composites

The XRD spectra of SR composites are shown in Figure 5(a,b). For the MT/SR composites, the clay (001) diffraction peak was shifted to lower angles as a result of a *d*-spacing increase. Generally, the driving force for polymer intercalation into the clay galleries results from the enthalpic contribution related to the establishment of many favorable polar polymer–surface interactions.[43] Thus, the increase in the *d*-spacing could be attributed to PDMS intercalation into the MT galleries, or more specifically, to the intercalation of segments of the PDMS chain ends, which

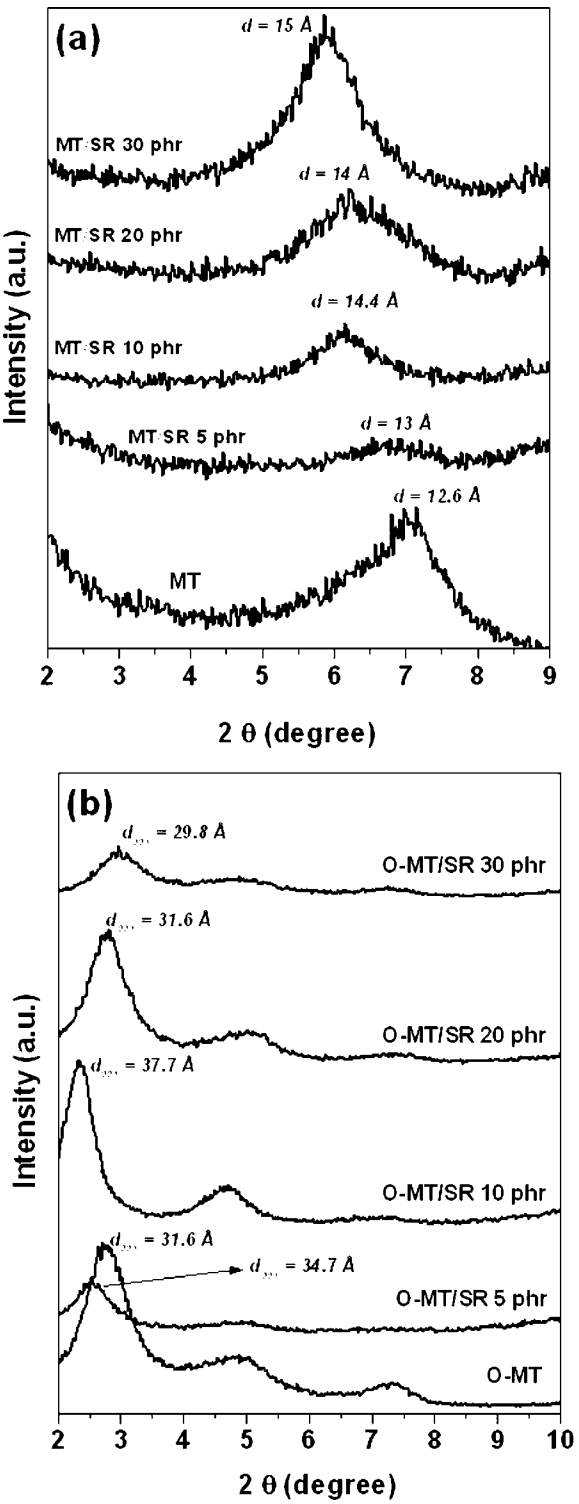

Figure 5 XRD patterns for the (a) MT and MT/SR and (b) O-MT and O-MT/SR composites.

contained $Si(CH_3)_2OH$ groups. These end groups could be associated with Si—OH groups from the platelet surface, especially at the edges,[44] by hydrogen bonds. As shown in Figure 5(a), the *d*-spacing of the MT/SR composites showed a tendency to

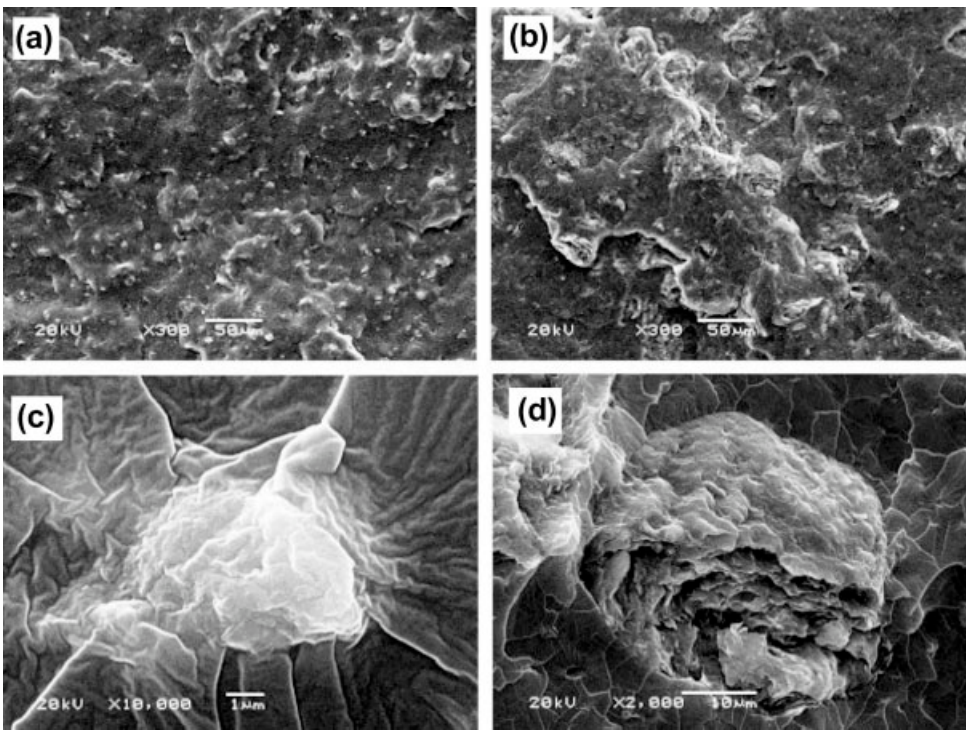

Figure 6 SEM micrographs of the (a,c) MT/SR and (b,d) O-MT/SR composites.

increase with the clay content. This was expected because the increase in the clay content led to a more intense PDMS fragmentation and, thus, an increase in the amount of PDMS–$Si(CH_3)_2OH$.

Figure 5(b) shows the XRD patterns for the O-MT/SR composites. The O-MT composite filled with 10 phr O-MT clay showed a more pronounced effect. As most polar sites of O-MT are not available for polymer interaction, the increase in *d*-spacing in this formulation could have been related to the diffusion of a peroxide byproduct from the radical initiator into the gallery space.

Morphology of the clay–rubber composites

The morphology of composites is often considered to be of crucial importance for the mechanical performance. The cryogenic fracture surfaces of the MT/SR and O-MT/SR composites, observed by SEM, are shown in Figures 6(a,c) and 6(b,d), respectively, which were typical of each composite set. The characteristics of particulate-filled composites are generally determined by the properties of each component, the composition, the distribution of the filler in the matrix, particle–particle interactions (agglomeration), and particle–matrix interactions (wetting and adhesion). For both clay–PDMS composite sets, the clays were uniformly distributed in the PDMS matrices. The micrographs also showed that the agglomeration of the clay particles was more evident in the O-MT filled composites. The size of the clay agglomerates in the clay–rubber composites reflected the nature of the filler–matrix interface. In the MT composites, the MT–PDMS covalent interface led to smaller and denser clay agglomerates wrapped up in PDMS matrix, as shown in Figure 6(a,c). On the other hand, in the O-MT filled composites, the weak and nonpolar nature of the clay–polymer interface did not promote reduction of the agglomerates, even when the low attractive forces among the particles produced by the presence of alkyl ammonium ions were considered. Figure 6(d) shows the porous O-MT agglomerate in the O-MT–PDMS composites. Despite the different natures of the filler–polymer interfaces, both clays showed good adhesion with the PDMS matrix. Figure 6(c) shows that MT was still covered by the PDMS matrix on the fracture surface, which agreed with the proposal of a covalent interface for the MT/SR composites.

Mechanical properties of the clay–rubber composites

The effect of clay introduction on the mechanical properties of PDMS rubber composites was analyzed, and the results are summarized in Figures 7 and 8. As expected, USR (0 phr) showed poor mechanical properties. The low mechanical performance of silicone rubbers in the unfilled state was attributed to the very low melting point ($\sim -45^{\circ}C$) of

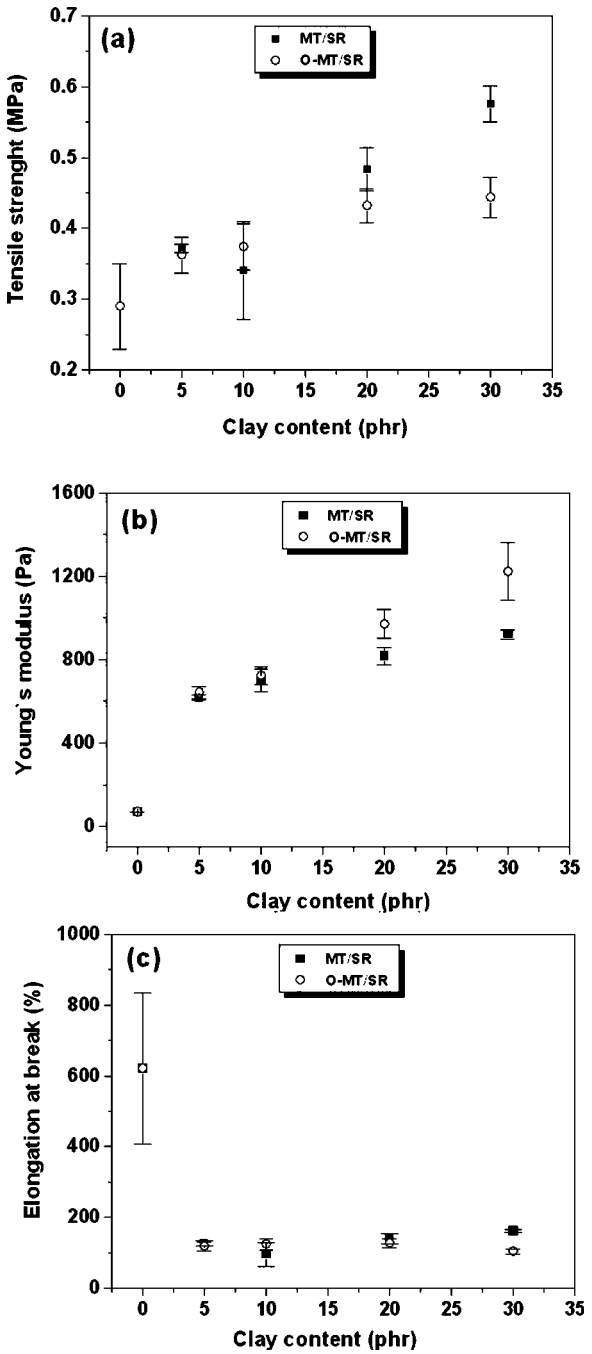

Figure 7 Mechanical properties of the USR and SR composites: (a) tensile strength, (b) Young's modulus, and (c) elongation at break.

PDMS, which could not readily provide a strain-induced crystallization[45] and, consequently, stronger interactions between chains. The SR composites showed a significant improvement in the tensile properties compared to the USR.

The dependence of composite tensile strength on the filler type and loading is shown in Figure 7(a). The tensile strength increased with the filler loading for both clays. The reinforcement effect, regardless of tensile strength, can be achieved by an efficient matrix–filler stress transfer, which can be obtained by a good adhesion at the filler–matrix interface.[46] Many mechanisms can contribute to good adhesion at interfaces, such as adsorption and weathering, interdiffusion, electrostatic attraction, chemical bonds, and mechanical adhesion. In general, weathering and chemical bonds are the most efficient mechanisms of reinforcement.[47] The formation of a covalent interface greatly contributed to tensile strength improvements in the MT/SR composites, in which MT acted as a chemical crosslinking junction. The tensile strength increased 27% for MT/SR 5 phr, in relation to USR rubber, and 96% for MT/SR 30 phr. For the O-MT/SR composites, the reinforcement mechanism was related to adsorption and weathering. The tensile strength also increased for O-MT/SR 5 phr and O-MT/SR 30 phr, in relation to USR rubber, by 24 and 52%, respectively. The difference between MT and O-MT filled PDMS on the tensile strength values was shown in the high-loaded composites (20 and 30 phr), where MT promoted a better reinforcement effect than O-MT due to the high number of covalent bonds at the MT–PDMS interface. However, the morphology of the rubber composites was mainly formed by agglomerates of clay particles, which is typical of microcomposite materials. For the rubber composites loaded with 5 phr clay, the obtained morphology, together with the relatively low amount of clay, justified the low mechanical performances.

The relationship between filler type and loading on the elastic modulus of the composites is shown in Figure 7(b). The increase in the elastic modulus in the SR composites indicated that the clays imparted some stiffness to the PDMS matrix. The elastic modulus depends strongly on the distribution of the filler (agglomerates or primary particles) in the polymeric

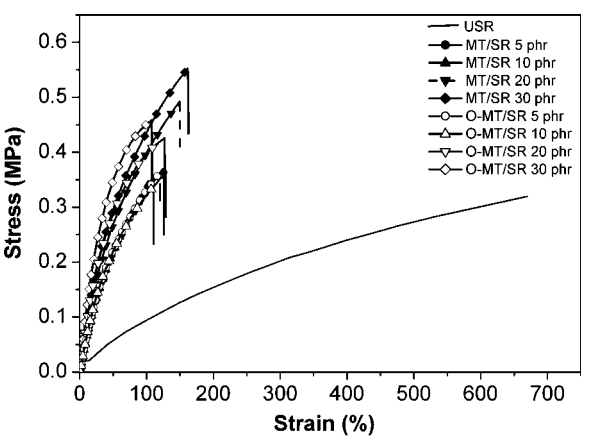

Figure 8 Stress–strain curves for the USR and SR composites.

matrix. The stress (and the resulting strain) used to determine the modulus is too small to separate agglomerated particles, and therefore, modulus enhancement is not significantly affected by particle agglomeration, as long as an uniform distribution of the filler into the matrix is ensured.[5] In addition to depending on the filler distribution (agglomerates or primary particles) in the matrix, modulus enhancement depends on the aspect ratio and volume fraction of the particles, in a similar way to that implied by the Halpin–Tsai equation.[48] The agglomerations of the MT and O-MT particles (as observed in the fracture morphologies of the composites) led to many complex shapes and sizes and, ultimately, to a distribution of aspect ratios. Consequently, it was difficult to evaluate the distinct modulus behavior between the MT/SR and O-MT/SR composites filled with 20 and 30 phr of clay. At intermediate strains, the increase in stiffness in the MT/SR composites was also a consequence of the increase in the crosslinking density arising from the polymer–filler bonds.[10]

The effect of the filler type and loading on the elongation at break of the composites is shown in Figure 7(c). Compared to USR, a significant decrease in the elongation at break was found for SR composites. This behavior has also been observed for other high-molar-mass PDMS filled composites[5,6] and could be attributed to the restricted deformation imposed by the filler. Even for the low-content-filled PDMS composites (5 phr of MT or O-MT), the elongation at break was drastically reduced.

CONCLUSIONS

In this article, clay–PDMS composites were prepared by a compounding/molding process with MT and O-MT. The two kinds of clay had distinct influences on the PDMS network:

1. MT increased the crosslinking density of PDMS rubbers, whereas O-MT decreased it.
2. Evidence of PDMS intercalation was found in the MT/SR composites, and the increase in the basal space of MT was enhanced with clay content in SR as well as with the crosslinking density. In contrast, in the O-MT/SR composites, the lack of polarity of O-MT restricted the PDMS intercalation.
3. The stronger filler–matrix interaction in MT/SR as composites reduced the size of clay agglomerates compared to that of the organically modified clay in the O-MT/SR composites. Moreover, both clays enhanced the thermal stability and the mechanical properties of PDMS with regard to tensile strength and modulus.

The authors thank Dow Corning do Brazil for providing the PDMS matrix. They also thank Carol H. Collins [Instituto de Quimica, Universidade Estadual de Campinas (IQ-UNICAMP)] for the manuscript revision.

References

1. Brydson, J. A. In Rubbery Materials and Their Compounds; Kluwer Academic Pub: Dordrecht, 1988; Chapter 13.
2. Dvornic, P. R.; Lenz R. W. In High Temperature Siloxane Elastomers; CIP: New York, 1990; Chapter 2.
3. Elvers, B.; Hawkins, S.; Russey, W.; Schulz G. In Ulmann's Encyclopedia of Industrial Chemistry, 5th ed.; VHC: New York, 1993; Vol. A24, Chapter 4.
4. Bokobza, L. J Appl Polym Sci 2004, 93, 2095.
5. Osman, M.; Atallah, A.; Kahr, G.; Suter, U. W. J Appl Polym Sci 2002, 83, 2175.
6. Silva, V. P.; Gonçalves, M. C.; Yoshida, I. V. P. J Appl Polym Sci 2006, 101, 290.
7. Redondo, S. U. A.; Gonçalves, M. C.; Yoshida, I. V. P. J Appl Polym Sci 2003, 89, 3739.
8. Burnside, S. D.; Giannelis, E. P. Chem Mater 1995, 7, 1597.
9. Burnside, S. D.; Giannelis, E. P. J. Polym Sci Part B: Polym Phys 2000, 38, 1595.
10. Bokobza, L. J Appl Polym Sci 2004, 93, 2095.
11. Takeuchi, H.; Cohen, C. Macromolecules 1999, 32, 6792.
12. Schmidt, D. F.; Clément, F.; Giannelis, E. P. Adv Funct Mater 2006, 16, 417.
13. Osman, M.; Atallah, A.; Kahr, G.; Suter, U. W. J Appl Polym Sci 2002, 83, 2175.
14. Annual Book of ASTM Standards; American Society for Testing and Materials: West Conshohocken, PA, 1998; ASTM D 471-98.
15. Annual Book of ASTM Standards; American Society for Testing and Materials: West Conshohocken, PA, 1998; ASTM D 412-98.
16. Venaruzzo, J. L.; Volzone, C.; Rueda, M. L.; Ortiga, J. Micropor Mesopor Mater 2002, 56, 73.
17. Khatib, K.; Pons, C. H.; Bottero, J. Y.; François, M.; Baudin, I. J Colloid Interface Sci 1995, 172, 317.
18. Altin, O.; Ozbelge, H. O.; Dogu, T. J Colloid Interface Sci 1999, 217, 19.
19. Gullick, R. W.; Weber, W. J., Jr. Environ Sci Technol 2001, 35, 1523.
20. Kaplan, D. L.; Serne, R. J.; Parker, K. E.; Kutnyakov, I. V. Environ Sci Technol 2000, 34, 399.
21. El-Akkad, T. M.; Flex, N. S.; Guindy, N. M.; El Massry, S. R.; Nashed, S. Surf Technol 1982, 17, 69.
22. Helmy, A. K.; Ferreiro, E. A.; Bussetti, S. G. D. J. J Colloid Interface Sci 1999, 210, 167.
23. Khalaf, H.; Bouras, O.; Perrichon, V. Micropour Mater 1997, 8, 141.
24. Wibulswas, R. Sep Purif Technol 2004, 39, 3.
25. Farmer, V. C. The Layer Silicates. In The Infrared Spectra of Minerals; Mineralogical Society, V. C.: London, 1974; p 331.
26. Yuquin, L.; Ishida, H. Langmuir 2003, 19, 2479.
27. Guggenhem, S.; van Groos, K. Clay Clay Miner 2001, 49, 433.
28. Song, S.; Sandí, G. Clay Clay Miner 2001, 49, 119.
29. Le Pluart, L.; Duchet, J.; Sautereau, H.; Gérard, J. F. J Adhes 2002, 78, 645.
30. Xie, W.; Gao, Z.; Pan, W. P.; Hunter, D.; Singh, A.; Vaia, R. Chem Mater 2001, 13, 2979.
31. Hauser, R. L. C.; Walker, A.; Kilbourne, F. L. Ind Eng Chem 1956, 48, 1202.
32. Sobhy, M. S.; Mahdy, M. M. M.; El-Fayoumi, M. A. K.; Abdel-Bary, E. M. Polym Test 1997, 16, 349.
33. Barton, A. F. M. In CRC Handbook of Solubility Parameters and Other Cohesion Parameters, 3rd ed.; CRC, Boca Raton, FL, 1985; Chapter 13.

34. Sereda, L.; Visconte, L. L. Y.; Nunes, R. C. R.; Furtado, C. R.; Riande, G. E. J Appl Polym Sci 2003, 90, 421.
35. Song, M.; Wong, C. W.; Jin, J.; Ansarifar, A.; Zhang, Z. Y.; Richardson, M. Polym Int 2005, 54, 560.
36. Chang, Y. W.; Yang, Y.; Ryu, S.; Nah, C. Polym Int 2002, 51, 319.
37. Kong, Q.; Hu, Y.; Song, L.; Wang, Y. Polym Adv Technol 2006, 17, 463.
38. Camino, G.; Lomakin, S. M.; Lazzari, M. Polymer 2001, 42, 2395.
39. Clarson, S. J.; Semlyen, J. A. In Siloxane Polymers; PTR Prentice Hall: New Jersey, 1993; Chapter 5.
40. Camino, G.; Lomakin, S. M.; Lageardm M. Polymer 2002, 43, 2011.
41. Camini, G.; Lomalin, S. M.; Lazzari, M. Polymer 2001, 42, 2395.
42. Xie, W.; Gao, Z.; Pan, W. P.; Hunter, D.; Singh, A.; Vaia, R. Chem Mater 2001, 13, 2979.
43. Vaia, R.; Giannelis, E. Macromolecules 1997, 30, 7990.
44. Van Olphen, H. In An Introduction to Clay Colloid Chemistry; Wiley: New York, 1963; Chapter 5.
45. Sharaf, M. A.; Kloczkowski, A.; Mark, J. E. Rubber Chem Technol 1995, 68, 601.
46. Kelly, A.; Zweben, C. In Comprehensive Composite Materials; Elsevier: Oxford, 2000; Vol. 2, Chapter 9.
47. Rabelo, M. In Aditivação de Polímeros; Artliber: São Paulo, Brazil, 2000; Chapter 10.
48. Halpin, J. C. J Compos Mater 1969, 3, 732.